Finite size effects on a cracked magnetoelectroelastic layer sandwiched between two elastic layers

ARTICLE *in* ENGINEERING FRACTURE MECHANICS · SEPTEMBER 2013

Impact Factor: 1.77 · DOI: 10.1016/j.engfracmech.2013.08.003

2 AUTHORS, INCLUDING:

Zengtao Chen
University of Alberta
144 PUBLICATIONS **1,173** CITATIONS

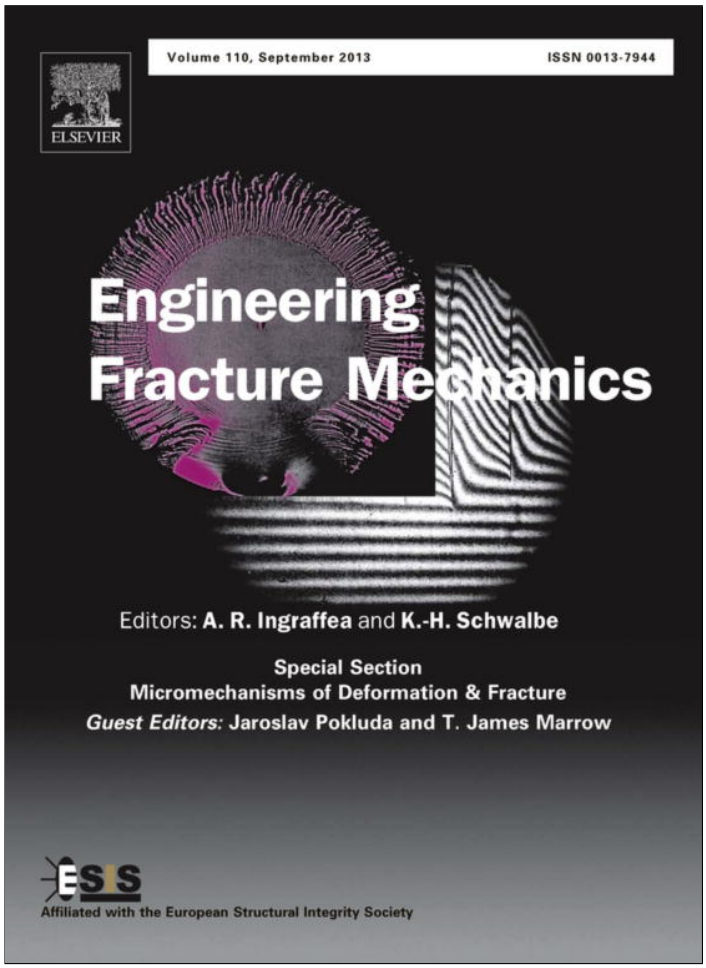

Engineering Fracture Mechanics 110 (2013) 23–37

Contents lists available at ScienceDirect

Engineering Fracture Mechanics

journal homepage: www.elsevier.com/locate/engfracmech

Finite size effects on a cracked magnetoelectroelastic layer sandwiched between two elastic layers

K.Q. Hu *, Z.T. Chen

Department of Mechanical Engineering, University of New Brunswick, Fredericton, NB E3B 5A3, Canada

ARTICLE INFO

Article history:
Received 28 November 2012
Received in revised form 30 July 2013
Accepted 3 August 2013
Available online 14 August 2013

Keywords:
Finite size effects
Magnetoelctroelastic layer
Fredholm integral equations
Field intensity factor

ABSTRACT

The crack problem of a magnetoelectroelastic layer of finite size sandwiched between two elastic layers under anti-plane shear and in-plane electric and magnetic loads is considered for impermeable and permeable crack surface conditions, respectively. Fourier transforms and Fourier sine series are used to reduce the mixed boundary value problem of the crack to dual integral equations, which are expressed in terms of Fredholm integral equations of the second kind. The stress field, electric field and magnetic field near the crack tip are obtained asymptotically, and the corresponding field intensity factors for impermeable and permeable cracks are determined. Numerical results show that the stress intensity factors, the electric displacement intensity factors and the magnetic induction intensity factors are influenced by the electric and magnetic loadings and the material properties. The finite size effects on the fracture behavior of the composite structure are investigated.

1. Introduction

Composites made of piezoelectric and piezomagnetic materials exhibit magnetoelectric effects that are not present in single-phase piezoelectric or piezomagnetic materials. Studies on the properties of piezoelectric/piezomagnetic composites have been carried out [1,2]. Defects or flaws may usually be introduced during the manufacturing process or during service by the external loading. These defects can result in the concentration of stress, electric displacement and magnetic induction, and further may lead to degradation failure. To secure the structural integrity of the piezoelectric/piezomagnetic composites, a better understanding of the field distributions around defects in the structure is prerequisite.

In recent decades, there is a growing interest among researchers in solving fracture mechanics problems in media possessing coupled piezoelectric, piezomagnetic and magnetoelectric effects, the magnetoelectroelastic effects. The crack initiation behaviors in a magnetoelectroelastic composite under in-plane deformation have been investigated in Sih and Song [3]. Wang and Mai [4] considered the mode III crack problem in an infinite piezoelectromagnetic medium by using complex variable techniques. The crack problem in a magnetoelectroelastic strip under longitudinal shear is studied in [5]. Li [6] analyzed the transient response of a cracked magnetoelectroelastic medium under antiplane mechanical and inplane electric and magnetic impacts. Moving crack problems in magnetoelectroelastic materials have been solved for an infinite magnetoelectroelastic body [7,8]. A closed-form solution of a mode-III crack in a magnetoelectroelastic layer was obtained and the crack face electromagnetic boundary conditions were discussed in [9]. Zhou et al. [10] studied mode-III edge-crack in magnetoelectroelastic media by sympletic expansion method. The researchers [11–14] have analyzed the penny-shaped crack problems in magnetoelectroelastic materials. Zhou and Chen [15] analyzed a mode-I limited-permeable crack in functionally graded piezoelectric/piezomagnetic materials subjected to a stress loading. Li and Lee [16] studied collinear unequal crack

* Corresponding author. Tel./fax: +1 5064587104.
E-mail addresses: keqianghu@163.com, ckhu@unb.ca (K.Q. Hu).

0013-7944/$ - see front matter © 2013 Elsevier Ltd. All rights reserved.
http://dx.doi.org/10.1016/j.engfracmech.2013.08.003

series in magnetoelectroelastic materials under mode-I loadings via real fundamental solutions. The dynamic behavior of a rectangular limited-permeable crack in magnetoelectroelastic media under an incident harmonic stress wave has been investigated by Zhang [17]. Fracture of magnetoelectroelastic composite materials has been considered by using boundary element method by García-Sanchez et al. [18].

Magnetoelectroelastic materials are inherently brittle and prone to cracking and study of the fracture behavior of a magnetoelectroelastic layer bonded to elastic layers is essential for the security and integrity of smart structures, as the bonded layers can improve the strength of the composite structures. The crack problem of a magnetoelectroelastic layer bonded to dissimilar half spaces employing the permeable crack surface conditions was considered in [19]. Su and Feng [20] investigated the fracture behavior of a bonded magneto-electro-elastic rectangular plate with an interface crack by employing the finite Fourier transform method.

For practical applications, the medium and the crack are always of finite size and the study of the fracture of finite size body is of great importance. The work in [21] presented results for the fracture of a rectangular magnetoelectroelastic body under anti-plane shear and in-plane electric and magnetic loadings. The effect of interfacial cracks on the magnetoelectric coupling properties of a magneto-electro-elastic composite laminate of finite size has been studied [22]. To the best knowledge of the authors, a cracked rectangular magnetoelectroelastic layer sandwiched between two elastic layers of finite size has not been reported due to the complexity of the material and boundary conditions.

The objective of this paper is to study the impermeable and permeable crack problems in a finite size magnetoelectroelastic layer sandwiched between two elastic layers under anti-plane mechanical and in-plane electric and magnetic loading. Fourier transforms and Fourier sine series are applied to reduce the mixed boundary value problem to dual integral equations, which can be expressed in terms of Fredholm integral equations of the second kind. The stress, electric, and magnetic fields near the crack tip are obtained asymptotically, the field intensity factors are defined and the effect of material properties, geometric size, and magnetic-electric loadings are analyzed. Closed form solutions based on impermeable and permeable crack surface conditions are obtained and the results are compared.

2. Basic equations for magnetoelectroelastic and elastic media

Consider a linear magnetoelectroelastic material which is assumed to be transversely isotropic and denote the rectangular coordinates of a point by $x_j (j = 1,2,3)$. The equilibrium equations are given as

$$\sigma_{ij,i} = 0, \quad D_{i,i} = 0, \quad B_{i,i} = 0 \tag{1}$$

where σ_{ij}, D_i and B_i are components of stress, electrical displacement and magnetic induction, respectively; a comma followed by $i (i = 1,2,3)$ denotes partial differentiation with respect to the coordinate x_i, and the usual summation convention over repeated indices is applied. The constitutive equations can be written as

$$\begin{aligned} \sigma_{ij} &= c_{ijks}\varepsilon_{ks} - e_{sij}E_s - h_{sij}H_s \\ D_i &= e_{iks}\varepsilon_{ks} + \lambda_{is}E_s + \beta_{is}H_s \\ B_i &= h_{iks}\varepsilon_{ks} + \beta_{is}E_s + \gamma_{is}H_s \end{aligned} \tag{2}$$

where ε_{ks}, E_s and H_s are components of strain, electric field and magnetic field, respectively; c_{ijks}, e_{iks}, h_{iks} and β_{is} are elastic, piezoelectric, piezomagnetic and electromagnetic constants, respectively; λ_{is} and γ_{is} are dielectric permitivities and magnetic permeabilities, respectively. The following reciprocal symmetries hold:

$$\begin{aligned} &c_{ijks} = c_{jiks} = c_{ijsk} = c_{ksij}, \quad e_{sij} = e_{sji} \\ &h_{sij} = h_{sji}, \quad \beta_{ij} = \beta_{ji}, \quad \lambda_{ij} = \lambda_{ji}, \quad \gamma_{ij} = \gamma_{ji} \end{aligned} \tag{3}$$

The gradient equations are

$$\varepsilon_{ij} = \frac{1}{2}(u_{i,j} + u_{j,i}), \quad E_i = -\phi_{,i}, \quad H_i = -\varphi_{,i} \tag{4}$$

where u_i is the displacement vector, ϕ and φ are the scalar electric and magnetic potentials, respectively. It is noted that Maxwell's vector equations in the quasi-static approximation are satisfied if the electric and magnetic fields are expressed as gradients of the scalar electric and magnetic potentials ϕ and φ, respectively [23], as shown in Eq. (4).

The governing equations simplify considerably if we consider only the out-of-plane displacement, the in-plane electric fields and in-plane magnetic fields, i.e.,

$$u_x = u_y = 0, \quad u_z = u_z(x,y) \tag{5}$$

$$E_x = E_x(x,y), \quad E_y = E_y(x,y), \quad E_z = 0 \tag{6}$$

$$H_x = H_x(x,y), \quad H_y = H_y(x,y), \quad H_z = 0 \tag{7}$$

$$u_x^E = u_y^E = 0, \quad u_z^E = u_z^E(x,y) \tag{8}$$

where the superscript "E" denote the quantities of the elastic layer, and similar definitions are applied through the paper.

The constitutive equations for anti-plane magnetoelectroelastic material take the form

$$\begin{pmatrix}\sigma_{zy}\\ D_y\\ B_y\end{pmatrix}=\begin{pmatrix}c_{44} & e_{15} & h_{15}\\ e_{15} & -\lambda_{11} & -\beta_{11}\\ h_{15} & -\beta_{11} & -\gamma_{11}\end{pmatrix}\begin{pmatrix}\frac{\partial u_z}{\partial y}\\ \frac{\partial \phi}{\partial y}\\ \frac{\partial \varphi}{\partial y}\end{pmatrix},\quad \begin{pmatrix}\sigma_{zx}\\ D_x\\ B_x\end{pmatrix}=\begin{pmatrix}c_{44} & e_{15} & h_{15}\\ e_{15} & -\lambda_{11} & -\beta_{11}\\ h_{15} & -\beta_{11} & -\gamma_{11}\end{pmatrix}\begin{pmatrix}\frac{\partial u_z}{\partial x}\\ \frac{\partial \phi}{\partial x}\\ \frac{\partial \varphi}{\partial x}\end{pmatrix}, \tag{9}$$

In this case, the governing Eq. (1) are simplified to

$$\begin{aligned} &c_{44}\nabla^2 u_z + e_{15}\nabla^2\phi + h_{15}\nabla^2\varphi = 0\\ &e_{15}\nabla^2 u_z - \lambda_{11}\nabla^2\phi - \beta_{11}\nabla^2\varphi = 0\\ &h_{15}\nabla^2 u_z - \beta_{11}\nabla^2\phi - \gamma_{11}\nabla^2\varphi = 0, \end{aligned} \tag{10}$$

The governing equation and constitutive equations of the elastic layers under anti-plane shear follow

$$\nabla^2 u_z^E = 0 \tag{11}$$

$$\sigma_{zy}^E = c_{44}^E\frac{\partial u_z^E}{\partial y},\quad \sigma_{zx}^E = c_{44}^E\frac{\partial u_z^E}{\partial x} \tag{12}$$

where $\nabla^2 = \partial^2/\partial x^2 + \partial^2/\partial y^2$ is the two-dimensional Laplacian operator in terms of x and y.

3. Problem statement and method of solution

Consider a central crack of length $2c$ in a rectangular magnetoelectroelastic layer sandwiched between two rectangular elastic layers with an elastic stiffness constant c_{44}^E, as shown in Fig. 1. The height and the width of the magnetoelectroelastic layer is $2d$ and $2h$, respectively, and the width of the elastic layer is $\Delta h = H - h$, with the height equal to that of the magnetoelectroelastic layer. The poling direction of the magnetoelectroelastic layer is oriented in the z-axis. It is assumed the geometric size in the thickness direction is big enough to permit the anti-plane stress state. The cracked structure is under anti-plane shear T_0 and in-plane electric field E_0 and magnetic field H_0 and the crack surfaces are traction-free. Theoretically, other possible combined loading conditions [4,5] can be dealt with in similar manners. In general case, the crack may occur at arbitrary location in the magnetoelectroelastic layer. The assumption of the symmetry made in this paper is for simplicity and so the problem may be solved without too much complexity and the insight and understanding of the coupling effect between elastic layer and the cracked magnetoelectroelastic layer can be observed.

It is noted that the elastic layers do not exhibit any piezoelectric or magnetostrictive properties, and the dielectric and diamagnetic properties of the elastic layers are assumed to be small compared to those of the magnetoelectroelastic material. In the present work, the effect of the electric and magnetic fields inside the elastic layers on the cracked composite is omitted.

The crack surfaces are assumed to be either electrically and magnetically impermeable or electrically and magnetically permeable. A coordinate system (x,y,z) is set at the center of the crack for reference. Considering the assumed symmetry in geometry and loading conditions, it is sufficient to consider the problem for $0 \leqslant x < H$, $0 \leqslant y < d$ only.

The electrical and magnetic boundary conditions for the magnetoelectroelastic layer are

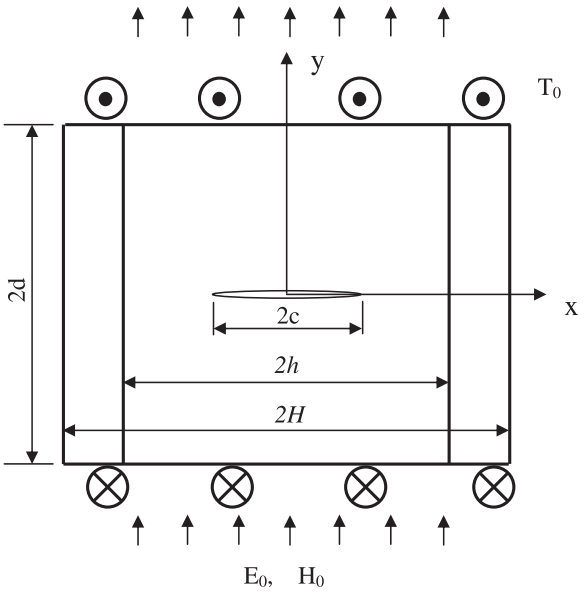

Fig. 1. A cracked rectangular magnetoelectroelastic layer sandwiched between two elastic layers under anti-plane shear T_0 and in-plane magnetic and electric loads H_0, E_0.

$$E_y(x,d)=E_0,\ H_y(x,d)=H_0 \quad (0\leqslant x\leqslant h) \tag{13}$$
$$D_x(h,y)=0,\ B_x(h,y)=0 \quad (0\leqslant y\leqslant d) \tag{14}$$

According to the symmetry to the x-axis and y-axis, the mechanical boundary conditions for the crack problem are

$$\sigma_{zx}(0,y)=0 \quad (0\leqslant y\leqslant d) \tag{15}$$
$$\sigma^E_{zx}(H,y)=0 \quad (0\leqslant y\leqslant d) \tag{16}$$
$$u^E_z(x,0)=0 \quad (h\leqslant x\leqslant H) \tag{17}$$
$$\sigma_{zy}(x,d)=T_0 \quad (0\leqslant x\leqslant h) \tag{18}$$
$$\sigma^E_{zy}(x,d)=T_0 \quad (h\leqslant x\leqslant H) \tag{19}$$
$$\sigma_{zy}(x,0)=0 \quad (0\leqslant x<c) \tag{20}$$
$$u_z(x,0)=0 \quad (c\leqslant x\leqslant h) \tag{21}$$

The continuity of displacement and stress on the interface of the elastic layer and the magnetoelectroelastic layer requires

$$u_z(h,y)=u^E_z(h,y) \quad (0\leqslant y\leqslant d) \tag{22}$$
$$\sigma_{zx}(h,y)=\sigma^E_{zx}(h,y) \quad (0\leqslant y\leqslant d) \tag{23}$$

Following the procedure in Chang [24] and Kwon and Lee [25], Fourier cosine transform and Fourier sine series are applied to Eqs. (10) and (11) and the appropriate expressions can be obtained as

$$u_z(x,y)=\frac{2}{\pi}\int_0^\infty A_1(\xi)\frac{\cosh[\xi(d-y)]}{\cosh(\xi d)}\cos(\xi x)d\xi+\sum_{n=0}^{\infty}B_1(n)\cosh(\beta_n x/d)\sin(\beta_n y/d)+a_0 y \tag{24}$$

$$\phi(x,y)=\frac{2}{\pi}\int_0^\infty A_2(\xi)\frac{\cosh[\xi(d-y)]}{\cosh(\xi d)}\cos(\xi x)d\xi+\sum_{n=0}^{\infty}B_2(n)\cosh(\beta_n x/d)\sin(\beta_n y/d)+b_0 y \tag{25}$$

$$\varphi(x,y)=\frac{2}{\pi}\int_0^\infty A_3(\xi)\frac{\cosh[\xi(d-y)]}{\cosh(\xi d)}\cos(\xi x)d\xi+\sum_{n=0}^{\infty}B_3(n)\cosh(\beta_n x/d)\sin(\beta_n y/d)+c_0 y \tag{26}$$

$$u^E_z(x,y)=\sum_{n=0}^{\infty}B_4(n)\cosh[\beta_n(H-x)/d]\sin(\beta_n y/d)+d_0 y \tag{27}$$

where $\beta_n=(2n+1)\pi/2$, $A_i(\xi)(i=1,2,3)$ and $B_j(n)(j=1,2,3,4)$ are the unknowns to be solved, and a_0, b_0,c_0 and d_0 are real constants which can be determined by considering the far-field and interface conditions, as given in Appendix A.

A simple calculation leads to the expressions for the stress, electric displacement and magnetic induction as:

$$\sigma_{zx}(x,y)=-\frac{2}{\pi}\int_0^\infty \xi[c_{44}A_1(\xi)+e_{15}A_2(\xi)+h_{15}A_3(\xi)]\frac{\cosh[\xi(d-y)]}{\cosh(\xi d)}\sin(\xi x)d\xi+\sum_{n=0}^{\infty}[c_{44}B_1(n)+e_{15}B_2(n)+h_{15}B_3(n)]\frac{\beta_n}{d}\sinh\left(\frac{\beta_n x}{d}\right)\sin\left(\frac{\beta_n y}{d}\right) \tag{28}$$

$$\sigma_{zy}(x,y)=-\frac{2}{\pi}\int_0^\infty \xi[c_{44}A_1(\xi)+e_{15}A_2(\xi)+h_{15}A_3(\xi)]\frac{\sinh[\xi(d-y)]}{\cosh(\xi d)}\cos(\xi x)d\xi+\sum_{n=0}^{\infty}[c_{44}B_1(n)+e_{15}B_2(n)+h_{15}B_3(n)]\frac{\beta_n}{d}\cosh\left(\frac{\beta_n x}{d}\right)\cos\left(\frac{\beta_n y}{d}\right)+T_0 \tag{29}$$

$$D_x(x,y)=-\frac{2}{\pi}\int_0^\infty \xi[e_{15}A_1(\xi)-\lambda_{11}A_2(\xi)-\beta_{11}A_3(\xi)]\frac{\cosh[\xi(d-y)]}{\cosh(\xi d)}\sin(\xi x)d\xi+\sum_{n=0}^{\infty}[e_{15}B_1(n)-\lambda_{11}B_2(n)-\beta_{11}B_3(n)]\frac{\beta_n}{d}\sinh\left(\frac{\beta_n x}{d}\right)\sin\left(\frac{\beta_n y}{d}\right) \tag{30}$$

$$D_y(x,y)=-\frac{2}{\pi}\int_0^\infty \xi[e_{15}A_1(\xi)-\lambda_{11}A_2(\xi)-\beta_{11}A_3(\xi)]\frac{\sinh[\xi(d-y)]}{\cosh(\xi d)}\cos(\xi x)d\xi+\sum_{n=0}^{\infty}[e_{15}B_1(n)-\lambda_{11}B_2(n)-\beta_{11}B_3(n)]\frac{\beta_n}{d}\cosh\left(\frac{\beta_n x}{d}\right)\cos\left(\frac{\beta_n y}{d}\right)+D_0 \tag{31}$$

$$B_x(x,y) = -\frac{2}{\pi}\int_0^\infty \xi[h_{15}A_1(\xi) - \beta_{11}A_2(\xi) - \gamma_{11}A_3(\xi)]\frac{\cosh[\xi(d-y)]}{\cosh(\xi d)}\sin(\xi x)d\xi + \sum_{n=0}^{\infty}[h_{15}B_1(n) - \beta_{11}B_2(n) - \gamma_{11}B_3(n)]\frac{\beta_n}{d}\sinh\left(\frac{\beta_n x}{d}\right)\sin\left(\frac{\beta_n y}{d}\right) \tag{32}$$

$$B_y(x,y) = -\frac{2}{\pi}\int_0^\infty \xi[h_{15}A_1(\xi) - \beta_{11}A_2(\xi) - \gamma_{11}A_3(\xi)]\frac{\sinh[\xi(d-y)]}{\cosh(\xi d)}\cos(\xi x)d\xi + \sum_{n=0}^{\infty}[h_{15}B_1(n) - \beta_{11}B_2(n) - \gamma_{11}B_3(n)]\frac{\beta_n}{d}\cosh\left(\frac{\beta_n x}{d}\right)\cos\left(\frac{\beta_n y}{d}\right) + B_0 \tag{33}$$

$$\sigma_{zx}^E = -\sum_{n=0}^{\infty}\frac{\beta_n}{d}c_{44}^E B_4(n)\sinh\left(\frac{\beta_n(H-x)}{d}\right)\sin\left(\frac{\beta_n y}{d}\right) \tag{34}$$

$$\sigma_{zy}^E = \sum_{n=0}^{\infty}\frac{\beta_n}{d}c_{44}^E B_4(n)\cosh\left(\frac{\beta_n(H-x)}{d}\right)\cos\left(\frac{\beta_n y}{d}\right) + T_0 \tag{35}$$

where D_0 and B_0 are constants defined in Appendix A.

It is obvious that the boundary conditions (15)–(19) are satisfied automatically when the appropriate stress and displacement expressions are substituted into (15)–(19). Eq. (13) are satisfied by considering the expressions in Eqs. (25) and (26). Satisfaction of Eqs. (14), (22) and (23) leads to the relations as follows

$$\sum_{n=0}^{\infty}\frac{\beta_n}{d}[e_{15}B_1(n) - \lambda_{11}B_2(n) - \beta_{11}B_3(n)]\sinh\left(\frac{\beta_n h}{d}\right)\sin\left(\frac{\beta_n y}{d}\right) = \frac{2}{\pi}\int_0^\infty \xi[e_{15}A_1(\xi) - \lambda_{11}A_2(\xi) - \beta_{11}A_3(\xi)]\frac{\cosh[\xi(d-y)]}{\cosh(\xi d)}\sin(\xi h)d\xi \tag{36}$$

$$\sum_{n=0}^{\infty}\frac{\beta_n}{d}[h_{15}B_1(n) - \beta_{11}B_2(n) - \gamma_{11}B_3(n)]\sinh\left(\frac{\beta_n h}{d}\right)\sin\left(\frac{\beta_n y}{d}\right) = \frac{2}{\pi}\int_0^\infty \xi[h_{15}A_1(\xi) - \beta_{11}A_2(\xi) - \gamma_{11}A_3(\xi)]\frac{\cosh[\xi(d-y)]}{\cosh(\xi d)}\sin(\xi h)d\xi \tag{37}$$

$$\sum_{n=0}^{\infty}\left[B_4(n)\cosh\left(\frac{\beta_n\Delta h}{d}\right) - B_1(n)\cosh\left(\frac{\beta_n h}{d}\right)\right]\sin\left(\frac{\beta_n y}{d}\right) = \frac{2}{\pi}\int_0^\infty A_1(\xi)\frac{\cosh[\xi(d-y)]}{\cosh(\xi d)}\cos(\xi h)d\xi + (a_0 - d_0)y \tag{38}$$

$$\sum_{n=0}^{\infty}\frac{\beta_n}{d}\left\{[c_{44}B_1(n) + e_{15}B_2(n) + h_{15}B_3(n)]\sinh\left(\frac{\beta_n h}{d}\right) + c_{44}^E B_4(n)\sinh\left(\frac{\beta_n\Delta h}{d}\right)\right\}\sin\left(\frac{\beta_n y}{d}\right) = \frac{2}{\pi}\int_0^\infty \xi[c_{44}A_1(\xi) + e_{15}A_2(\xi) + h_{15}A_3(\xi)]\frac{\cosh[\xi(d-y)]}{\cosh(\xi d)}\sin(\xi h)d\xi \tag{39}$$

With the help of the Fourier sine pair [26]

$$f(y) = \sum_{n=0}^{\infty}B(n)\sin\left(\frac{(2n+1)\pi y}{2d}\right)$$
$$B(n) = \frac{2}{d}\int_0^d f(y)\sin\left(\frac{(2n+1)\pi y}{2d}\right)dy \tag{40}$$

and the identity [27] (see also in Appendix B)

$$\int_0^d \cosh[\xi(d-y)]\sin(\beta y)dy = \frac{\beta}{\xi^2+\beta^2}[\cosh(\xi d) - \cos(\beta d)] \tag{41}$$

The relations between the unknown functions $B_j(n)(j = 1,2,3,4)$ and the unknown functions $A_i(\xi)(i = 1,2,3)$ can be obtained from Eqs. (36)–(39) as:

$$[e_{15}B_1(n) - \lambda_{11}B_2(n) - \beta_{11}B_3(n)]\sinh\frac{\beta_n h}{d} = \frac{4}{\pi d}\int_0^\infty \xi[e_{15}A_1(\xi) - \lambda_{11}A_2(\xi) - \beta_{11}A_3(\xi)]\frac{\sin(\xi h)}{\xi^2 + (\beta_n/d)^2}d\xi \tag{42}$$

$$[h_{15}B_1(n) - \beta_{11}B_2(n) - \gamma_{11}B_3(n)]\sinh\left(\frac{\beta_n h}{d}\right) = \frac{4}{\pi d}\int_0^\infty \xi[h_{15}A_1(\xi) - \beta_{11}A_2(\xi) - \gamma_{11}A_3(\xi)]\frac{\sin(\xi h)}{\xi^2 + (\beta_n/d)^2}d\xi \tag{43}$$

$$B_4(n)\cosh\frac{\beta_n\Delta h}{d}-B_1(n)\cosh\left(\frac{\beta_n h}{d}\right)=\frac{4}{\pi d}\int_0^\infty\frac{\beta_n}{d}A_1(\xi)\frac{\cos(\xi h)}{\xi^2+(\beta_n/d)^2}d\xi+\frac{2d(a_0-d_0)}{\beta_n^2}\sin(\beta_n) \tag{44}$$

$$\begin{aligned}&[c_{44}B_1(n)+e_{15}B_2(n)+h_{15}B_3(n)]\sinh\left(\frac{\beta_n h}{d}\right)+c_{44}^E B_4(n)\sinh\left(\frac{\beta_n\Delta h}{d}\right)\\&=\frac{4}{\pi d}\int_0^\infty\xi[c_{44}A_1(\xi)+e_{15}A_2(\xi)+h_{15}A_3(\xi)]\frac{\sin(\xi h)}{\xi^2+(\beta_n/d)^2}d\xi\end{aligned} \tag{45}$$

By solving Eqs. (42)–(45), functions $B_j(n)(j=1,2,3,4)$ can be expressed in terms of functions $A_i(\xi)(i=1,2,3)$ as

$$B_j(n)=f_j(A_1(\xi),A_2(\xi),A_3(\xi),n)\quad(j=1,2,3,4) \tag{46}$$

where functions $f_j(A_1(\xi),A_2(\xi),A_3(\xi),n)$ are given in Appendix A.

3.1. Electrically and magnetically impermeable crack assumption

Considering the fact that the electric and magnetic constants of magnetoelectroelastic materials are large and are on the order of a few thousand times the electric and magnetic permittivities of air or vacuum inside the crack, the impermeable electric and magnetic boundary conditions along the crack face may be assumed [4,5]

$$D_y(x,0)=0\quad(0\leqslant x<c) \tag{47}$$
$$\phi(x,0)=0\quad(c\leqslant x\leqslant h) \tag{48}$$
$$B_y(x,0)=0\quad(0\leqslant x<c) \tag{49}$$
$$\varphi(x,0)=0\quad(c\leqslant x\leqslant h) \tag{50}$$

A system of dual integral equations can be obtained from the mixed boundary conditions (20) and (21) and (47)–(50) as

$$\int_0^\infty\xi A_i(\xi)\cos(x\xi)\tanh(\xi d)d\xi-\frac{\pi}{2}\sum_{n=0}^\infty\frac{\beta_n}{d}\cosh(x\beta_n/d)B_i(n)=\frac{\pi}{2}\Omega_i\quad(0\leqslant x<c) \tag{51}$$

$$\int_0^\infty A_i(\xi)\cos(\xi x)d\xi=0\quad(c\leqslant x\leqslant h)\quad(i=1,2,3) \tag{52}$$

where the constants Ω_i are defined as $\Omega_1=a_0$, $\Omega_2=b_0$,$\Omega_3=c_0$.

Substituting $B_j(n)(j=1,2,3)$ from Eq. (46) into Eq. (51), we can get

$$\begin{aligned}&\frac{d}{dx}\int_0^\infty A_i(\xi)\sin(\xi x)d\xi+\int_0^\infty\xi A_i(\xi)[\tanh(\xi d)-1]\cos(\xi x)d\xi\\&-\frac{\pi}{2}\sum_{n=0}^\infty f_i(A_1(\xi),A_2(\xi),A_3(\xi),n)\frac{\beta_n}{d}\cosh\frac{\beta_n x}{d}=\frac{\pi}{2}\Omega_i\quad(0\leqslant x<c)\end{aligned} \tag{53}$$

By introducing three auxiliary functions $\Phi_i(\zeta)$ $(i=1,2,3)$ as

$$A_i(\xi)=\frac{\pi}{2}\Omega_i c^2\int_0^1\zeta\Phi_i(\zeta)J_0(\xi c\zeta)d\zeta \tag{54}$$

where $J_0(\,)$ is the zero-order Bessel function of the first kind, it can be found that Eq. (52) are satisfied automatically by considering the identity

$$\int_0^\infty J_0(\xi t)\cos(\xi x)d\xi=\begin{cases}0, & |x|>t\\(t^2-x^2)^{-1/2}, & |x|<t\end{cases} \tag{55}$$

and functions $\Phi_i(t)$ $(i=1,2,3)$ can be determined by the following simultaneous Fredholm integral equations [28–30]

$$\Phi_i(t)+\sum_{j=1}^3\int_0^1\Phi_j(\eta)K_{ij}(\eta,t)d\eta=F_i(t)\quad(i=1,2,3) \tag{56}$$

where the known functions $F_i(t)$ $(i=1,2,3)$ and the kernel functions $K_{ij}(\eta,t)$ $(i,j=1,2,3)$ are defined in Appendix A.

In the limit case that $h\to\infty$ and $c_{44}^E=0$, the kernels $K_{ij}(\eta,t)=0$, $(i\neq j)$ and $F_i(t)=1$, we can get the solution for an infinite magnetoelectroelastic strip with a central crack parallel to the boundary [5], and the corresponding Fredholm integral equations are reduced to the form

$$\Phi_i(t)+\int_0^1\Phi_i(\eta)K(\eta,t)d\eta=1\quad(i=1,2,3) \tag{57}$$

where the kernel function is

$$K(\eta,t)=\zeta\int_0^\infty \xi[\tanh(\xi d/c)-1]J_0(\xi\zeta)J_0(\xi t)d\xi \tag{58}$$

When $d\to\infty$ and $c_{44}^E=0$, the kernels $K_{ij}(\eta,t)=0$, $(i\neq j)$, $F_i(t)=1$, and by assuming that $\lim_{d\to\infty}(\pi/d)=d\xi$, $\beta_n/d=\xi$; the solution for an infinite magnetoelectroelastic strip with a crack vertical to the boundaries can be reduced from Eq. (56), the corresponding integral equations are

$$\Phi_i(t)+\sum_{j=1}^{3}\int_0^1 \Phi_j(\eta)H(\eta,t)d\eta=1\quad(i=1,2,3) \tag{59}$$

where the kernel functions $H(\eta,t)$ is in the form as

$$H(\zeta,t)=\zeta\int_0^\infty \xi[1-\coth(\xi h/c)]I_0(\xi\zeta)I_0(\xi t)d\xi \tag{60}$$

where $I_0(\,)$ is the modified zero-order Bessel function of the first kind. The expression (60) is in agreement with Chen and Meguid [31] for the case of a vertical crack in an infinite piezoelectric strip.

If $h\to\infty$ and $d\to\infty$, the kernels $K_{ij}(\eta,t)=0$ and $F_i(t)=1$, and we can get the solution from Eq. (56) as $\Phi_i(t)\equiv 1(i=1,2,3)$, which corresponds to the exact solution for an infinite magnetoelectroelastic body with a crack under anti-plane shear and in-plane electric and magnetic loading [4].

3.2. Electrically and magnetically permeable crack assumption

For an electrically and magnetically permeable crack, the upper and lower surfaces of the crack are electrically and magnetically contacted, and the electrical potential and the magnetic potential vanish everywhere on the crack faces [9], i.e.,

$$\phi(x,0)=0,\ \ \varphi(x,0)=0\quad(0\leqslant x\leqslant h) \tag{61}$$

These equations show that Eqs. (48) and (50) are valid for both the impermeable and permeable crack assumptions.

In this case $A_2(\xi)=A_3(\xi)=0$ and $A(\xi)=A_1(\xi)$ is the only unknown function to be solved. Dual integral equations about the permeable crack problem can be obtained from the mixed boundary conditions in (20) and (21) as

$$\begin{aligned}&\int_0^\infty \xi A(\xi)\tanh(\xi d)\cos(\xi x)d\xi\\&-\frac{\pi}{2}\sum_{n=0}^{\infty}\frac{\beta_n}{d}\left[B_1(n)+\frac{e_{15}}{c_{44}}B_2(n)+\frac{h_{15}}{c_{44}}B_3(n)\right]\cosh\frac{\beta_n x}{d}=\frac{\pi}{2}f_0\quad(0\leqslant x<c)\end{aligned} \tag{62}$$

$$\int_0^\infty A(\xi)\cos(\xi x)d\xi=0\quad(c\leqslant x\leqslant h) \tag{63}$$

where the constant $f_0=T_0/c_{44}$.

By introducing an auxiliary function $\Psi(t)$, the unknown function $A(\xi)$ can be expressed as

$$A(\xi)=\frac{\pi}{2}f_0c^2\int_0^1 t\Psi(t)J_0(\xi ct)dt \tag{64}$$

where the function $\Psi(t)$ can be obtained by solving the following Fredholm integral equation

$$\Psi(t)+\int_0^1 \Psi(\eta)P(\eta,t)d\eta=E(t) \tag{65}$$

where the known function $E(t)$ and the kernel function $P(\eta,t)$ are defined in Appendix A.

4. Near-tip fields and field intensity factors

The Fredholm integral Eqs. (56) and (65) can be numerically solved by using the collocation method. Once the functions $\Phi_i(t)$ $(i=1,2,3)$ and $\Psi(t)$ are obtained, following the procedure in Chen and Sih [32], the functions $A_i(\xi)(i=1,2,3)$ and $A(\xi)$ can be expressed as

$$A_i(\xi)=\frac{\pi\Omega_i}{2\xi}c\left\{\Phi_i(1)J_1(\xi c)-\int_0^1 tJ_1(\xi ct)\frac{d}{dt}[\Phi_i(t)]dt\right\}\quad(i=1,2,3) \tag{66}$$

$$A(\xi)=\frac{\pi f_0}{2\xi}c\left\{\Psi(1)J_1(\xi c)-\int_0^1 tJ_1(\xi ct)\frac{d}{dt}[\Psi(t)]dt\right\} \tag{67}$$

where $J_1(\,)$ is the first-order Bessel function of the first kind.

From the point of view of fracture mechanics, only the singular field quantities around the crack tip are of interest, which will be derived here. The singular crack tip fields correspond to the behavior of the integrand as the integration variables ξ tends to infinity, which is fully described by the first term on the right hand side of Eqs. (66) and (67) containing $\Phi_i(1)$ ($i = 1,2,3$) and $\Psi(1)$.

The stress, electric and magnetic fields near the crack tip can be obtained by substituting Eqs. (66) and (67) into Eqs. (28)–(33). By considering the identity [27]

$$\int_0^\infty e^{-\alpha x} J_1(\beta x)dx = \frac{\sqrt{\alpha^2+\beta^2}-\alpha}{\beta\sqrt{\alpha^2+\beta^2}}, \quad (\mathrm{Re}(\alpha \pm i\beta) > 0) \tag{68}$$

the stresses, electric displacements and magnetic inductions near the crack tip can be obtained as

$$\sigma_{zy}(r,\theta) + i\sigma_{zx}(r,\theta) = \frac{K^T}{\sqrt{2\pi r}}\exp(-i\theta/2) + \mathrm{O}(r^0) \tag{69}$$

$$D_y(r,\theta) + iD_x(r,\theta) = \frac{K^D}{\sqrt{2\pi r}}\exp(-i\theta/2) + \mathrm{O}(r^0) \tag{70}$$

$$B_y(r,\theta) + iB_x(r,\theta) = \frac{K^B}{\sqrt{2\pi r}}\exp(-i\theta/2) + \mathrm{O}(r^0) \tag{71}$$

where r and θ are defined as

$$r = \sqrt{(x-c)^2+y^2}, \ \theta = \tan^{-1}\left(\frac{y}{x-c}\right) \tag{72}$$

For electrically and magnetically impermeable crack, the stress intensity factor (SIF) K^T, the electric displacement intensity factor (EDIF) K^D and the magnetic induction intensity factor (MIIF) K^B can be defined, respectively, as

$$K^T = \lim_{r\to 0^+}\sqrt{2\pi r}\sigma_{zy}(r,0) = [c_{44}a_0\Phi_1(1) + e_{15}b_0\Phi_2(1) + h_{15}c_0\Phi_3(1)]\sqrt{\pi c} \tag{73}$$

$$K^D = \lim_{r\to 0^+}\sqrt{2\pi r}D_y(r,0) = [e_{15}a_0\Phi_1(1) - \lambda_{11}b_0\Phi_2(1) - \beta_{11}c_0\Phi_3(1)]\sqrt{\pi c} \tag{74}$$

$$K^B = \lim_{r\to 0^+}\sqrt{2\pi r}B_y(r,0) = [h_{15}a_0\Phi_1(1) - \beta_{11}b_0\Phi_2(1) - \gamma_{11}c_0\Phi_3(1)]\sqrt{\pi c} \tag{75}$$

For the limit case when $h \to \infty$ and $d \to \infty$, we have $\Phi_i(t) \equiv 1$ ($i = 1,2,3$), and the field intensity factors K^T, K^D and K^B for an infinite magnetoelectroelastic body with an impermeable crack under anti-plane shear and in-plane electric and magnetic loading can be obtained as

$$K^T_\infty = [c_{44}a_0 + e_{15}b_0 + h_{15}c_0]\sqrt{\pi c} = T_0\sqrt{\pi c} \tag{76}$$

$$K^D_\infty = [e_{15}a_0 - \lambda_{11}b_0 - \beta_{11}c_0]\sqrt{\pi c} = D_0\sqrt{\pi c} \tag{77}$$

$$K^T_\infty = [h_{15}a_0 - \beta_{11}b_0 - \gamma_{11}c_0]\sqrt{\pi c} = B_0\sqrt{\pi c} \tag{78}$$

To analyze the effect of material constants, the loading conditions and the geometric size on the fracture behavior of the sandwiched structure, it is convenient to define the normalized field intensity factors as follows

$$K_T = K^T/K^T_\infty = [c_{44}a_0\Phi_1(1) + e_{15}b_0\Phi_2(1) + h_{15}c_0\Phi_3(1)]/T_0 \tag{79}$$

$$K_D = K^D/K^D_\infty = [e_{15}a_0\Phi_1(1) - \lambda_{11}b_0\Phi_2(1) - \beta_{11}c_0\Phi_3(1)]/D_0 \tag{80}$$

$$K_B = K^B/K^B_\infty = [h_{15}a_0\Phi_1(1) - \beta_{11}b_0\Phi_2(1) - \gamma_{11}c_0\Phi_3(1)]/B_0 \tag{81}$$

It should be noted that if the geometric size is finite, the normalized field intensity factors K_T, K_D and K_B are dependent on the loadings and the geometric sizes of the cracked rectangular magnetoelectroelastic layer and the bonded elastic layers.

For electrically and magnetically permeable crack, the SIF K^T, the EDIF K^D and the MIIF K^B can be defined, respectively, as

$$K^T = \lim_{r\to 0^+}\sqrt{2\pi r}\sigma_{zy}(r,0) = T_0\Psi(1)\sqrt{\pi c} \tag{82}$$

$$K^D = \lim_{r\to 0^+}\sqrt{2\pi r}D_y(r,0) = \frac{e_{15}}{c_{44}}K^T \tag{83}$$

$$K^B = \lim_{r\to 0^+}\sqrt{2\pi r}B_y(r,0) = \frac{h_{15}}{c_{44}}K^T \tag{84}$$

It is clear that for electrically and magnetically permeable crack, the EDIFs and MIIFs are solely determined in terms of the applied SIFs. This conclusion is in agreement with the results of Wang et al. [9].

5. Numerical results and discussions

To determine the field intensity factors, we need the values of functions $\Phi_i(1) = \Phi_i(x)|_{x=1}$ $(i = 1,2,3)$ for an impermeable crack and $\Psi(1) = \Psi(x)|_{x=1}$ for a permeable crack. The material properties of the magnetoelectroelastic layer is taken as a transversely isotropic material exhibiting full coupling between electric, magnetic and elastic fields, with a unique axis along the z-direction. The material constants used in the following numerical calculation are selected as [33]:

$$\begin{aligned} &c_{44} = 5.0 \times 10^{10}\ (\mathrm{N/m^2}), \quad e_{15} = 0.2\ (\mathrm{C/m^2}) \\ &\lambda_{11} = 2.5 \times 10^{-10}\ (\mathrm{C^2/Nm^2}), \quad \beta_{11} = 5.3 \times 10^{-9}\ (\mathrm{Ns/VC}) \\ &h_{15} = 180\ (\mathrm{N/Am}), \quad \gamma_{11} = -2.0 \times 10^{-6}\ (\mathrm{Ns^2/C^2}) \end{aligned} \tag{85}$$

To study the effect of magneto-electro-elastic interaction on the singular field near the crack tip, the loading parameters L_E and L_H are defined, respectively as:

$$L_E = e_{15}E_0/T_0, \ L_H = h_{15}H_0/T_0 \tag{86}$$

where L_E represents the ratio of electric load to mechanical load, and L_H represents the ratio of magnetic load to mechanical load.

To study the effect of material property and loading parameters on the field intensity factors, the geometric size of the composite structure is chosen as $d/c = h/c = 3, \Delta h = H - h = 0.1c$, without loss of generality. The numerical results of the normalized SIFs for the impermeable and permeable crack problems are presented and compared. In the following figures, "I" and "P" denote impermeable and permeable crack surface conditions, respectively.

Fig. 2 shows the variation of the normalized SIFs versus the material parameter ratio $R = c_{44}^E/c_{44}$ for different values of the electrical loading parameter L_E when $L_H = 0$. The SIFs increase or decrease as the ratio R increases, depending on the magnitude of the loading parameter L_E. When $L_E \geqslant 0$, the SIFs decreases as R increases; and the SIFs increases as R increases when L_E is smaller than a certain negative value (around -0.2). For $R = 0$, the normalized SIFs remain to be a constant when varying the loading parameters L_E, which corresponds to the case of a central crack in a magnetoelectroelastic body under anti-plane shear and in-plane electric and magnetic loading. Similar conclusions can be observed from Fig. 3, which shows the variation of the normalized SIFs with the material ratio R for different magnetic loading parameters L_H when $L_E = 0$. The normalized SIFs can be decreased either by decreasing R when L_H is smaller than a certain negative value; when L_H is positive, the normalized SIFs decrease with increasing the values of L_H or R. It can be seen from Figs. 2 and 3 that the results of the SIFs for the electrically and magnetically impermeable crack are very close to those for the permeable crack.

The effect of the geometric size ratio c/d on the normalized SIFs are shown in Fig. 4 for different values of material parameter ratio R when $h/c = 3$, $\Delta h/c = 0.1$ and $L_E = L_H = 0.5$. It can be observed that for a given geometric size d, K_T decreases as R increases. When R is larger than a certain value, K_T increases as the ratio c/d increases, i.e., the SIF increases as the height d decreases. If R is less than a certain value, K_T will decreases as the size d decreases and reaches a certain minimum value and then increases as d decreases. It can be seen that the elastic layers with higher R values have a tendency to decrease the stress intensity factor; and decreasing the size d has a tendency to increase K_T values. For the high values of d $(d > 5c)$, the normalized SIFs are almost constants, depending on different R values of the elastic layer. As d decreases below a certain value (say $c/d = 0.7$ for $R = 0.5$), the effect of decreasing the size d becomes dominant and K_T increases correspondingly.

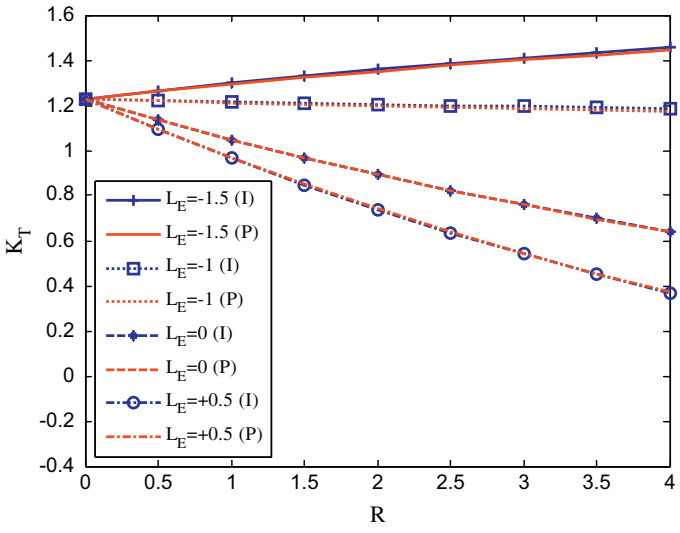

Fig. 2. Effect of $R = c_{44}^E/c_{44}$ on K_T for different values of L_E when $L_H = 0$.

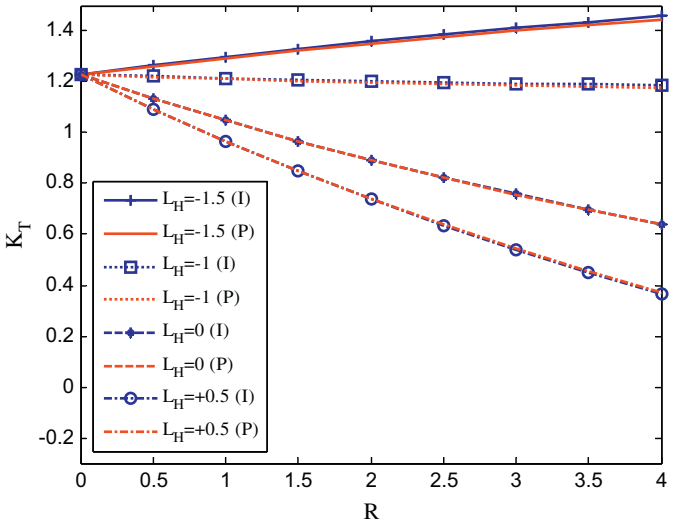

Fig. 3. Effect of $R = c_{44}^{E}/c_{44}$ on K_T for different values of L_H when $L_E = 0$.

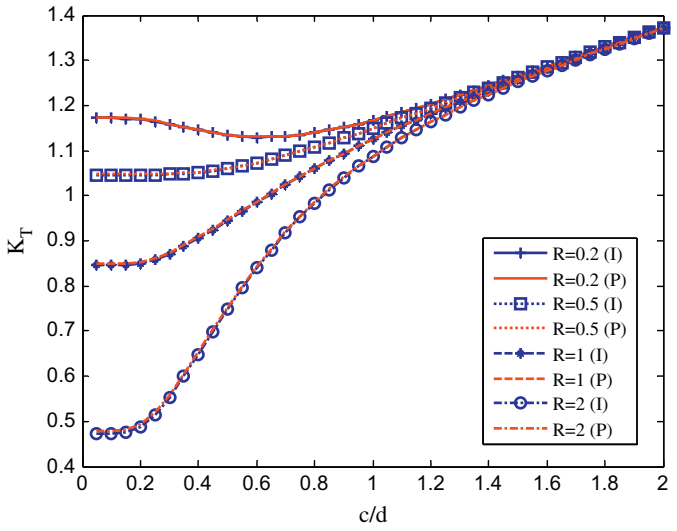

Fig. 4. Effect of c/d on K_T for different values of R.

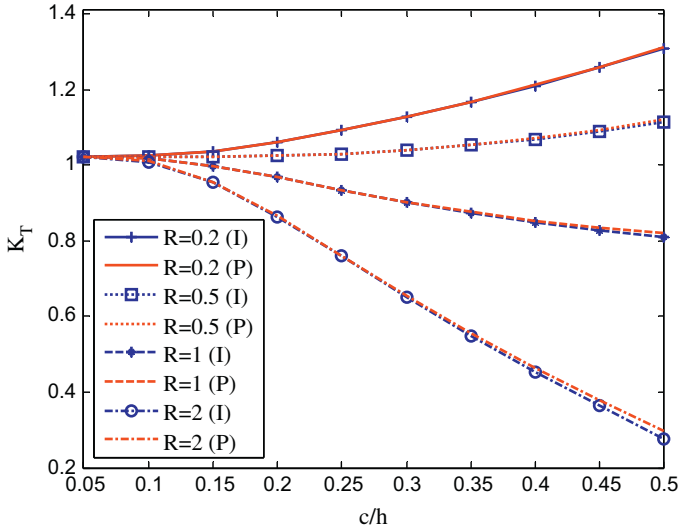

Fig. 5. Effect of c/h on K_T for different values of R.

Fig. 5 shows the variation of the normalized SIFs with the ratio c/h for different values of R when $d/c = 3, \Delta h/c = 0.1$ and $L_E = L_H = 0.5$. It can be observed that K_T increases as c/h increases when the value of R is smaller than a certain value, which implies that a decrease in h value can lead to an increase in K_T. When the value of R is bigger than a certain value, a decrease in h value can lead to a lower value of K_T. For the same value of c/h, K_T decreases as R increases, which indicates that R has the tendency to decrease the SIFs, as shown in Fig. 4. The difference of the values of K_T for impermeable crack and permeable crack is small when R is small and the difference becomes bigger as the value of R increases.

The variations of the normalized SIFs with the geometric size Δh are shown in Fig. 6 for different values of material parameter ratio R when $d/c = h/c = 3$ and $L_E = L_H = 0.5$. The SIFs increase as Δh increases when the material parameter ratio R is smaller than a certain value (say 0.45), and the SIFs decrease as Δh increases when R is bigger than a certain value. For the same Δh value, K_T decreases as R increases, which indicate that lower K_T values can be obtained by increasing R values. For bigger values of R, the difference of the results of K_T values for impermeable and permeable cracks become more obvious.

The effects of the electric and magnetic fields on the normalized electric displacement intensity factor (EDIF) K_D for different R values are displayed in Fig. 7a and Fig. 7b for the impermeable and permeable crack boundary conditions, respectively. The geometric size of the composite is assumed as $d/c = h/c = 3, \Delta h/c = 0.1$ and the EDIF is normalized by the electric displacement value D_0 corresponding to T_0 and $L_E = +1, L_H = 0$. For impermeable crack case, K_D increases as the electric field loading parameter L_E increases and the change of the material parameter R has a very mild effect on the variation of K_D, as shown in Fig. 7a. The variations of K_D with L_E for the permeable crack case are shown in Fig. 7b, which shows that K_D decreases as the parameter L_E increases, and the change of the material parameter R does affect the magnitude of K_D.

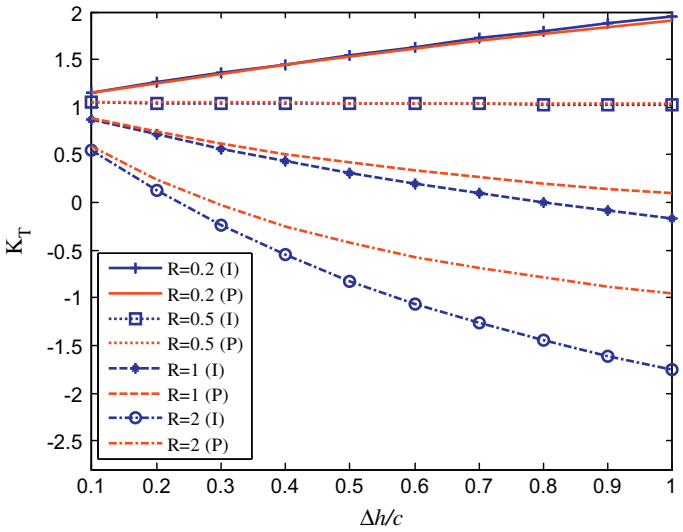

Fig. 6. Effect of $\Delta h/c$ on K_T for different values of R.

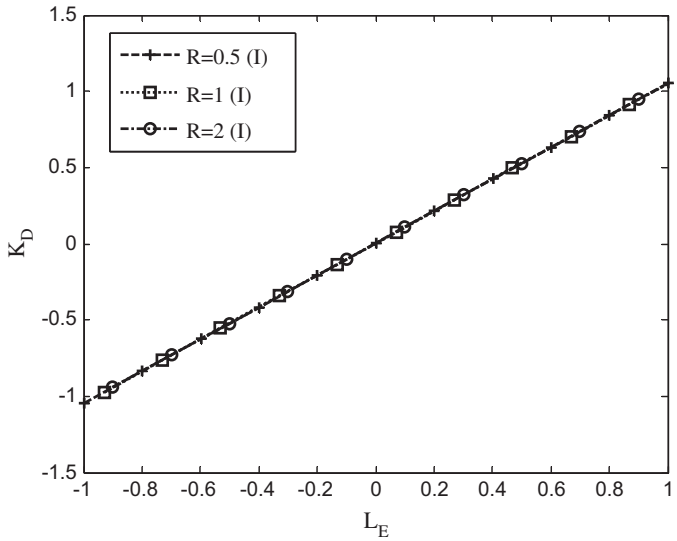

Fig. 7a. Effect of L_E on K_D for different values of R for impermeable crack when $L_H = 0$.

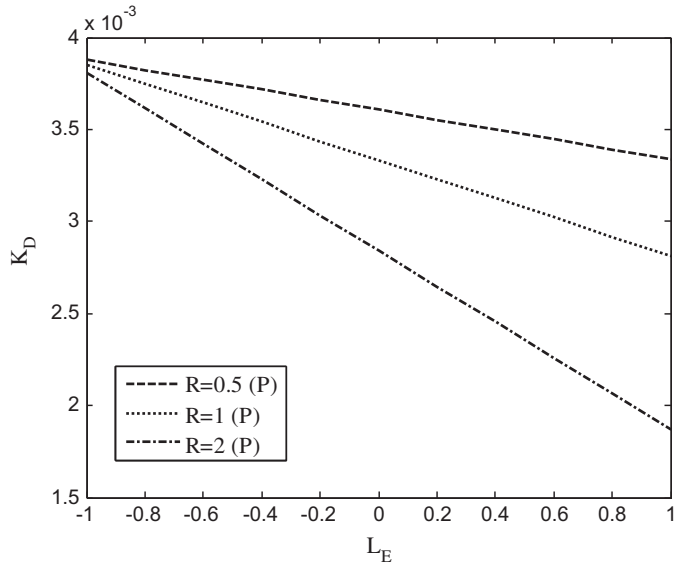

Fig. 7b. Effect of L_E on K_D for different values of R for permeable crack when $L_H = 0$.

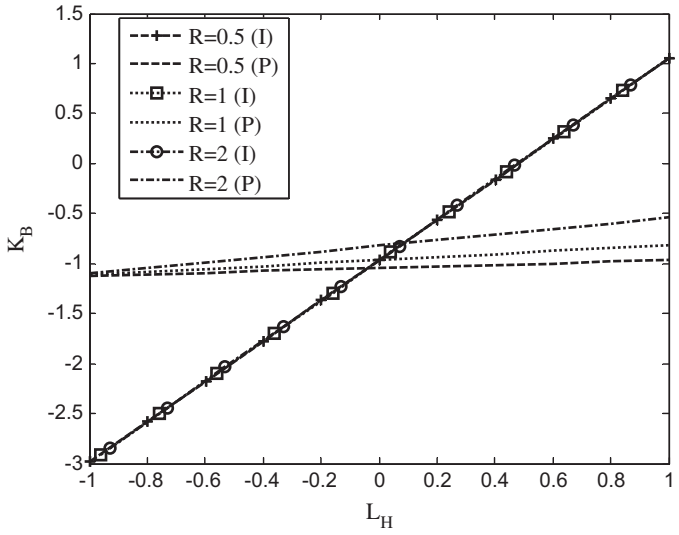

Fig. 8. Effect of L_H on K_B for different values of R when $L_E = 0$.

Fig. 8 shows the variations of the normalized magnetic induction intensity factor (MIIF) K_B with the magnetic loading parameter L_H when $d/c = h/c = 3, \Delta h/c = 0.1$ and $L_E = 0$. The MIIF is normalized by the magnetic induction value B_0 with the application of T_0 and $L_E = 0$, $L_H = +1$. K_B increases as the magnetic field loading parameter L_H increases and the results of K_B for different values of material parameter R are almost the same for the impermeable crack, while the change of R does affect the magnitude of K_B for the permeable crack case. It is noted that K_D and K_B are also affected by the geometric size of the cracked magnetoelectroelastic composite and the crack face boundary conditions.

6. Conclusions

A cracked rectangular magnetoelectroelastic layer sandwiched between two elastic layers under anti-plane shear and in-plane electric and magnetic loads is studied for impermeable and permeable crack surface boundary conditions, respectively. Fourier transforms and Fourier sine series are used to reduce the mixed boundary value problem of the crack to dual integral equations, which are expressed in terms of Fredholm integral equations of the second kind. The stress, electric, and magnetic fields near the crack tip are obtained, and the field intensity factors are defined accordingly. Numerical results show that the stress intensity factors are influenced by the electric and magnetic loadings, the material properties and the finite geometric size of the composite structure. The electric and magnetic fields have different effects on the electric displacement intensity factor and magnetic induction intensity factor for different crack face boundary conditions.

Appendix A

Constants a_0, b_0, c_0, d_0 are obtained by considering the far-field and interface conditions as

$$\begin{pmatrix} a_0 \\ b_0 \\ c_0 \end{pmatrix} = \begin{pmatrix} c_{44} & e_{15} & h_{15} \\ 0 & -1 & 0 \\ 0 & 0 & -1 \end{pmatrix}^{-1} \begin{pmatrix} T_0 \\ E_0 \\ H_0 \end{pmatrix} \tag{A.1-1}$$

$$d_0 = T_0/c_{44}^E \tag{A.1-2}$$

$$\begin{aligned} D_0 &= \frac{[e_{15}T_0 + (c_{44}\lambda_{11} + e_{15}^2)E_0 + (c_{44}\beta_{11} + e_{15}h_{15})H_0]}{c_{44}} \\ B_0 &= \frac{[h_{15}T_0 + (c_{44}\beta_{11} + e_{15}h_{15})E_0 + (c_{44}\gamma_{11} + h_{15}^2)H_0]}{c_{44}} \end{aligned} \tag{A.2}$$

Functions $f_j(A_1(\xi),A_2(\xi),A_3(\xi),n)$ $(j = 1,2,3)$ in Eq. (46) are defined as

$$f_j(A_1(\xi),A_2(\xi),A_3(\xi),n) = \frac{4}{\pi d}\left\{\begin{array}{l} \sum_{i=1}^{3}\int_0^\infty \frac{\xi A_i(\xi)\sin(\xi h)}{\xi^2+(\beta_n/d)^2}\cosh\frac{\beta_n\Delta h}{d}M_{ij}(n)d\xi \\ -\int_0^\infty \frac{A_1(\xi)\cos(\xi h)}{\xi^2+(\beta_n/d)^2}c_{44}^E b_{j1}(n)\frac{\beta_n}{d}\sinh\frac{\beta_n\Delta h}{d}d\xi \end{array}\right\} + B_{j0}(n) \tag{A.3}$$

where functions $M_{ij}(n)$ and $B_{j0}(n)$ $(i,j = 1,2,3)$ are defined respectively as

$$M_{1j}(n) = c_{44}b_{j1}(n) + e_{15}b_{j2}(n) + h_{15}b_{j3}(n) \tag{A.4-1}$$

$$M_{2j}(n) = e_{15}b_{j1}(n) - \lambda_{11}b_{j2}(n) - \beta_{11}b_{j3}(n) \tag{A.4-2}$$

$$M_{3j}(n) = h_{15}b_{j1}(n) - \beta_{11}b_{j2}(n) - \gamma_{11}b_{j3}(n) \tag{A.4-3}$$

$$B_{j0}(n) = b_{j1}R_0(n) \quad (j = 1,2,3) \tag{A.5}$$

$$R_0(n) = 2\frac{c_{44}^E(d_0 - a_0)d}{\beta_n^2}\sin(\beta_n)\sinh\left(\frac{\beta_n\Delta h}{d}\right) \tag{A.6}$$

$$b_{11}(n) = (\lambda_{11}\gamma_{11} - \beta_{11}^2)/\Delta(n) \tag{A.7-1}$$

$$b_{12}(n) = b_{21}(n) = (e_{15}\gamma_{11} - h_{15}\beta_{11})/\Delta(n) \tag{A.7-2}$$

$$b_{13}(n) = b_{31}(n) = (h_{15}\lambda_{11} - e_{15}\beta_{11})/\Delta(n) \tag{A.7-3}$$

$$b_{22}(n) = -\frac{c_{44}\gamma_{11} + h_{15}^2 + c_{44}^E\gamma_{11}\tanh(\beta_n\Delta h/d)/\tanh(\beta_n h/d)}{\Delta(n)} \tag{A.7-4}$$

$$b_{23}(n) = b_{32}(n) = \frac{c_{44}\beta_{11} + h_{15}e_{15} + c_{44}^E\beta_{11}\tanh(\beta_n\Delta h/d)/\tanh(\beta_n h/d)}{\Delta(n)} \tag{A.7-5}$$

$$b_{33}(n) = -\frac{c_{44}\lambda_{11} + e_{15}^2 + c_{44}^E\lambda_{11}\tanh(\beta_n\Delta h/d)/\tanh(\beta_n h/d)}{\Delta(n)} \tag{A.7-8}$$

$$\Delta(n) = (\lambda_{11}\gamma_{11} - \beta_{11}^2)Q_1(n) + (e_{15}\gamma_{11} - h_{15}\beta_{11})Q_2(n) + (h_{15}\lambda_{11} - e_{15}\beta_{11})Q_3(n) \tag{A.8}$$

$$Q_1(n) = c_{44}\sinh\left(\frac{\beta_n h}{d}\right)\cosh\left(\frac{\beta_n\Delta h}{d}\right) + c_{44}^E\cosh\left(\frac{\beta_n h}{d}\right)\sinh\left(\frac{\beta_n\Delta h}{d}\right) \tag{A.9-1}$$

$$Q_2(n) = e_{15}\sinh(\beta_n h/d)\cosh(\beta_n\Delta h/d) \tag{A.9-2}$$

$$Q_3(n) = h_{15}\sinh(\beta_n h/d)\cosh(\beta_n\Delta h/d) \tag{A.9-3}$$

Functions $F_i(t)$ $(i = 1,2,3)$ and the kernel functions $K_{ij}(\eta,t)$ $(i,j = 1,2,3)$ in Eq. (56) are defined, respectively, as:

$$F_1(t) = 1 + \frac{1}{a_0}\sum_{n=0}^{\infty}B_{10}(n)\frac{\beta_n}{d}I_0(\beta_n ct/d) \tag{A.10-1}$$

$$F_2(t) = 1 + \frac{1}{b_0}\sum_{n=0}^{\infty}B_{20}(n)\frac{\beta_n}{d}I_0(\beta_n ct/d) \tag{A.10-2}$$

$$F_3(t) = 1 + \frac{1}{c_0}\sum_{n=0}^{\infty}B_{30}(n)\frac{\beta_n}{d}I_0(\beta_n ct/d) \tag{A.10-3}$$

$$K_{11}(\zeta,t)=\zeta\int_0^\infty \xi[\tanh(\xi d/c)-1]J_0(\xi\zeta)J_0(\xi t)d\xi+\zeta\sum_{n=0}^{\infty}\frac{\pi\beta_n c^2}{d^2}c_{44}^E b_{11}(n)e^{-\beta_n h/d}\sinh\left(\frac{\beta_n\Delta h}{d}\right)I_0(\beta_n c\zeta/d)I_0(\beta_n ct/d)$$
$$-\zeta\sum_{n=0}^{\infty}\frac{\pi\beta_n c^2}{d^2}q_{11}(n)e^{-\beta_n h/d}\cosh\left(\frac{\beta_n\Delta h}{d}\right)I_0(\beta_n c\zeta/d)I_0(\beta_n ct/d) \tag{A.11}$$

$$\frac{K_{12}(\zeta,t)}{c^2}=-\frac{b_0}{a_0}\zeta\sum_{n=0}^{\infty}\frac{\pi\beta_n}{d^2}q_{12}(n)e^{-\beta_n h/d}\cosh\left(\frac{\beta_n\Delta h}{d}\right)I_0(\beta_n c\zeta/d)I_0(\beta_n ct/d) \tag{A.12}$$

$$\frac{K_{13}(\zeta,t)}{c^2}=-\frac{c_0}{a_0}\zeta\sum_{n=0}^{\infty}\frac{\pi\beta_n}{d^2}q_{13}(n)e^{-\beta_n h/d}\cosh\left(\frac{\beta_n\Delta h}{d}\right)I_0(\beta_n c\zeta/d)I_0(\beta_n ct/d) \tag{A.13}$$

$$\frac{K_{21}(\zeta,t)}{c^2}=-\frac{a_0\zeta}{b_0}\left\{\begin{array}{l}\sum_{n=0}^{\infty}\frac{\pi\beta_n}{d^2}e^{-\beta_n h/d}I_0\left(\frac{\beta_n c\zeta}{d}\right)I_0\left(\frac{\beta_n ct}{d}\right)q_{21}(n)\cosh\left(\frac{\beta_n\Delta h}{d}\right)\\ -\sum_{n=0}^{\infty}\frac{\pi\beta_n}{d^2}e^{-\beta_n h/d}I_0\left(\frac{\beta_n c\zeta}{d}\right)I_0\left(\frac{\beta_n ct}{d}\right)c_{44}^E b_{21}(n)\sinh\left(\frac{\beta_n\Delta h}{d}\right)\end{array}\right\} \tag{A.14}$$

$$K_{22}(\zeta,t)=\zeta\int_0^\infty \xi[\tanh(\xi d/c)-1]J_0(\xi c\zeta)J_0(\xi ct)d\xi-\zeta\sum_{n=0}^{\infty}\frac{\pi\beta_n c^2}{d^2}q_{22}(n)e^{-\beta_n h/d}\cosh\left(\frac{\beta_n\Delta h}{d}\right)I_0(\beta_n c\zeta/d)I_0(\beta_n ct/d) \tag{A.15}$$

$$\frac{K_{23}(\zeta,t)}{c^2}=-\frac{c_0}{b_0}\zeta\sum_{n=0}^{\infty}\frac{\pi\beta_n}{d^2}q_{23}(n)e^{-\beta_n h/d}\cosh\left(\frac{\beta_n\Delta h}{d}\right)I_0(\beta_n c\zeta/d)I_0(\beta_n ct/d) \tag{A.16}$$

$$\frac{K_{31}(\zeta,t)}{c^2}=-\frac{a_0}{c_0}\zeta\left\{\begin{array}{l}\sum_{n=0}^{\infty}\frac{\pi\beta_n}{d^2}e^{-\beta_n h/d}I_0\left(\frac{\beta_n c\zeta}{d}\right)I_0\left(\frac{\beta_n ct}{d}\right)q_{31}(n)\cosh\left(\frac{\beta_n\Delta h}{d}\right)\\ -\sum_{n=0}^{\infty}\frac{\pi\beta_n}{d^2}e^{-\beta_n h/d}I_0\left(\frac{\beta_n c\zeta}{d}\right)I_0\left(\frac{\beta_n ct}{d}\right)c_{44}^E b_{31}(n)\sinh\left(\frac{\beta_n\Delta h}{d}\right)\end{array}\right\} \tag{A.17}$$

$$\frac{K_{32}(\zeta,t)}{c^2}=-\frac{b_0}{c_0}\zeta\sum_{n=0}^{\infty}\frac{\pi\beta_n}{d^2}q_{32}(n)e^{-\beta_n h/d}\cosh\left(\frac{\beta_n\Delta h}{d}\right)I_0(\beta_n c\zeta/d)I_0(\beta_n ct/d) \tag{A.18}$$

$$K_{33}(\zeta,t)=\zeta\int_0^\infty \xi[\tanh(\xi d/c)-1]J_0(\xi c\zeta)J_0(\xi ct)d\xi-\zeta\sum_{n=0}^{\infty}\frac{\pi\beta_n c^2}{d^2}q_{33}(n)e^{-\beta_n h/d}\cosh\left(\frac{\beta_n\Delta h}{d}\right)I_0(\beta_n c\zeta/d)I_0(\beta_n ct/d) \tag{A.19}$$

Functions $q_{ij}(n)(i,j=1,2,3)$ are defined as

$$q_{i1}(n)=c_{44}b_{i1}(n)+e_{15}b_{i2}(n)+h_{15}b_{i3}(n) \tag{A.20-1}$$
$$q_{i2}(n)=e_{15}b_{i1}(n)-\lambda_{11}b_{i2}(n)-\beta_{11}b_{i3}(n) \tag{A.20-2}$$
$$q_{i3}(n)=h_{15}b_{i1}(n)-\beta_{11}b_{i2}(n)-\gamma_{11}b_{i3}(n) \tag{A.20-3}$$

Function $E(t)$ and the kernel functions $P(\eta,t)$ in Eq. (65) are

$$E(t)=1+\frac{1}{f_0}\sum_{n=0}^{\infty}\left[B_{10}(n)+\frac{e_{15}}{c_{44}}B_{20}(n)+\frac{h_{15}}{c_{44}}B_{30}(n)\right]\frac{\beta_n}{d}I_0(\beta_n ct/d) \tag{A.21}$$

$$P(\eta,t)=\eta\int_0^\infty \xi[\tanh(\xi d/c)-1]J_0(\xi c\eta)J_0(\xi ct)d\xi+\eta\sum_{n=0}^{\infty}\frac{\pi\beta_n c^2}{d^2}c_{44}^E\frac{q_{11}(n)}{c_{44}}e^{-\beta_n h/d}$$
$$\times\sinh\left(\frac{\beta_n\Delta h}{d}\right)I_0(\beta_n c\eta/d)I_0(\beta_n ct/d)-\eta\sum_{n=0}^{\infty}\frac{\pi\beta_n c^2}{d^2}\left[\frac{c_{44}q_{11}(n)+e_{15}q_{21}(n)+h_{15}q_{31}(n)}{c_{44}}\right]e^{-\beta_n h/d}$$
$$\times\cosh\left(\frac{\beta_n\Delta h}{d}\right)I_0\left(\frac{\beta_n c\eta}{d}\right)I_0\left(\frac{\beta_n ct}{d}\right) \tag{A.22}$$

Appendix B

Use the identity in [27] (pp. 196)

$$\int\exp(ax)\sin(bx)dx=\frac{\exp(ax)[a\sin(bx)-b\cos(ax)]}{a^2+b^2} \tag{B.1}$$

The following identity stands

$$\begin{aligned}\int_0^d \cosh[\xi(d-y)]\sin(\beta y)dy &= \frac{1}{2}\int_0^d \{\exp[\xi(d-y)]+\exp[-\xi(d-y)]\}\sin(\beta y)dy \\ &= \frac{1}{2}\left[\exp(\xi d)\int_0^d \exp(-\gamma y)\sin(\beta y)dy + \exp(-\xi d)\int_0^d \exp(\gamma y)\sin(\beta y)dy\right] \\ &= \frac{1}{2}\frac{\beta[\exp(\xi d)+\exp(-\xi d)]-2\beta\cos(\beta d)}{\xi^2+\beta^2} \\ &= \frac{\beta}{\xi^2+\beta^2}[\cosh(\xi d)-\cos(\beta d)]\end{aligned} \tag{B.2}$$

References

[1] Nan CW. Magnetoelectric effect in composite of piezoelectric and piezomagnetic phases. Phys Rev B 1994;50:6082–8.
[2] Benveniste Y. Magnetoelectric effect in fibrous composites with piezoelectric and piezomagnetic phases. Phys Rev B 1995;51:16424–7.
[3] Sih GC, Song ZF. Magnetic and electric poling effects associated with crack growth in $BaTiO_3$–$CoFe_2O_4$ composite. Theor Appl Fract Mech 2003;39:209–27.
[4] Wang BL, Mai YW. Fracture of piezoelectromagnetic materials. Mech Res Commun 2004;31:65–73.
[5] Hu KQ, Li GQ. Electro-magneto-elastic analysis of a piezoelectro-magnetic strip with a finite crack under longitudinal shear. Mech Mater 2005;37:925–34.
[6] Li XF. Dynamic analysis of a cracked magnetoelectroelastic medium under antiplane mechanical and inplane electric and magnetic impacts. Int J Solids Struct 2005;42:3185–205.
[7] Hu KQ, Li GQ. Constant moving crack in a magnetoelctroelastic material under anti-plane shear loading. Int J Solids Struct 2005;42:2823–35.
[8] Tupholme GE. Moving antiplane shear crack in transversely isotropic magnetoelectroelastic media. Acta Mech 2007;202:153–62.
[9] Wang BL, Han JC, Mai YW. Mode III fracture of a magnetoelectroelastic layer: exact solution and discussion of the crack face electromagnetic boundary conditions. Int J Fract 2006;139:27–38.
[10] Zhou ZH, Xu XS, Leung AYT. Mode III edge-crack in magneto-electro-elastic media by symplectic expansion. Eng Fract Mech 2010;77:3157–73.
[11] Feng WJ, Pan E, Wang X. Dynamic fracture analysis of a penny-shaped crack in a magnetoelectroelastic layer. Int J Solids Struct 2007;44:7955–74.
[12] Tian WY, Rajapakse RKND. Field intensity factors of a penny-shaped crack in a magnetoelectroelastic layer. J Alloys Compd 2008;449:161–71.
[13] Zhong XC, Li XF. Fracture analysis of a magnetoelectroelastic body with a penny-shaped crack by considering the effects of the opening crack interior. Int J Engng Sci 2008;46:374–90.
[14] Zhao M-H, Yang F, Liu T. Analysis of a penny-shaped crack in magneto-electro-elastic medium. Philos Mag 2006;86:4397–416.
[15] Zhou ZG, Chen ZT. Basic solution of a Mode-I limited-permeable crack in functionally graded piezoelectric/piezomagnetic materials. Int J Solids Struct 2008;45:2265–96.
[16] Li YD, Lee KY. Collinear unequal crack series in magnetoelectroelastic materials: mode I case solved via new real fundamental solutions. Engng Fract Mech 2010;77:2772–90.
[17] Zhang PW. Dynamic fracture of a rectangular limited-permeable crack in magneto-electro-elastic media under a time-harmonic elastic P-wave. Int J Solids Struct 2011;48:553–66.
[18] García-Sanchez F, Rojas-Díaz R, Saez A, Zhang Ch. Fracture of magnetoelectroelastic composite materials using boundary element method (BEM). Theor Appl Fract Mech 2007;47:192–204.
[19] Hu KQ, Qin QH, Kang YL. Anti-plane shear crack in a magnetoelectroelastic layer sandwiched between dissimilar half spaces. Engng Fract Mech 2007;74:1139–47.
[20] Su RKL, Feng WJ. Fracture behavior of a bonded magneto-electro-elastic rectangular plate with an interface crack. Arch Appl Mech 2008;78:343–62.
[21] Hu KQ, Li GQ, Zhong Z. Fracture of a rectangular piezoelectromagnetic body. Mech Res Commun 2006;33:482–92.
[22] Wang BL, Han JC. Effect of finite cracking on the magneto-electric coupling properties of magneto-electro-elastic composite laminates. J Intel Mat Syst Str 2010;21:1669–79.
[23] Parton VZ, Kudryavtsev BA. Electromagnetoelasticity, piezoelectrics and electrically conductive solids. New York: Gordon and Breach; 1988.
[24] Chang SS. The solution of a rectangular orthotropic sheet with a central crack under anti-plane shear. Engng Fract Mech 1985;22:253–61.
[25] Kwon SM, Lee KY. Analysis of stress and electric fields in a rectangular piezoelectric body with a central crack under anti-plane shear loading. Int J Solids Struct 2000;37:4859–69.
[26] Sneddon IN. Fourier transforms. New York: McGraw-Hill; 1951.
[27] Gradshtegn IS, Ryzhik IM. Tables of integral series and products. New York: Academic Press; 1965.
[28] Copson ET. On certain dual integral equations. Proc Glasgow Math Assoc 1961;5:19–24.
[29] Westmann RA. Simultaneous pairs of dual integral equations. SIAM Rev 1965;7:341–8.
[30] Sih GC, Chen EP. Mechanics of fracture 6: cracks in composite materials. London: Martinus Nijhoff Publishers; 1981.
[31] Chen ZT, Meguid SA. The transient response of a piezoelectric strip with a vertical crack under electromechanical impact load. Int J Solids Struct 2000;37:6051–62.
[32] Chen EP, Sih GC. Interfacial delamination of a layered composite under anti-plane strain. J Compos Mater 1971;5:12–23.
[33] Buchanan GR. Layered versus multiphase magneto-electro-elastic composites. Composites: Part B 2004;35:413–20.